

## Article

# A High Flux Electrochemical Filtration System Based on Electrospun Carbon Nanofiber Membrane for Efficient Tetracycline Degradation

Xue Yang <sup>1,2</sup>, Xian Li <sup>1,2</sup>, Yongyou Hu <sup>1,2,\*</sup>, Jianhua Cheng <sup>1</sup> and Yuancai Chen <sup>1</sup>

<sup>1</sup> School of Environment and Energy, South China University of Technology, Guangzhou Higher Education Mega Centre, Guangzhou 510006, China; huanyin163@163.com (X.Y.); fit33335@126.com (X.L.); jhcheng@scut.edu.cn (J.C.); chenyc@scut.edu.cn (Y.C.)

<sup>2</sup> The Key Lab of Pollution Control and Ecosystem Restoration in Industry Clusters, Ministry of Education, South China University of Technology, Guangzhou Higher Education Mega Centre, Guangzhou 510006, China

\* Correspondence: ppyyhu@scut.edu.cn

**Abstract:** In this work, an electrochemical filter using an electrospun carbon nanofiber membrane (ECNFM) anode fabricated by electrospinning, stabilization and carbonization was developed for the removal of antibiotic tetracycline (TC). ECNFM with 2.5 wt% terephthalic acid (PTA) carbonized at 1000 °C (ECNFM-2.5%-1000) exhibited higher tensile stress (0.75 MPa) and porosity (92.8%), more graphitic structures and lower electron transfer resistance (23.52 Ω). Under the optimal condition of applied voltage 2.0 V, pH 6.1, 0.1 mol L<sup>-1</sup> Na<sub>2</sub>SO<sub>4</sub>, initial TC concentration 10 ppm and membrane flux 425 LMH, the TC removal efficiency of the electrochemical filter of ECNFM-2.5%-1000 reached 99.8%, and no obvious performance loss was observed after 8 h of continuous operation. The pseudo-first-order reaction rate constant in flow-through mode was 2.28 min<sup>-1</sup>, which was 10.53 times higher than that in batch mode. Meanwhile, the energy demand for 90% TC removal was only 0.017 kWh m<sup>-3</sup>. TC could be converted to intermediates with lower developmental toxicity and mutagenicity via the loss of functional groups (-CONH<sub>2</sub>, -CH<sub>3</sub>, -OH, -N(CH<sub>3</sub>)<sub>2</sub>) and ring opening reaction, which was mainly achieved by direct anodic oxidation. This study highlights the potential of ECNFM-based electrochemical filtration for efficient and economical drinking water purification.

**Keywords:** electrospun carbon nanofiber membrane; electrochemical filtration; tetracycline; drinking water



**Citation:** Yang, X.; Li, X.; Hu, Y.; Cheng, J.; Chen, Y. A High Flux Electrochemical Filtration System Based on Electrospun Carbon Nanofiber Membrane for Efficient Tetracycline Degradation. *Water* **2022**, *14*, 910. <https://doi.org/10.3390/w14060910>

Academic Editor: José Alberto Herrera-Melián

Received: 3 February 2022

Accepted: 9 March 2022

Published: 15 March 2022

**Publisher's Note:** MDPI stays neutral with regard to jurisdictional claims in published maps and institutional affiliations.



**Copyright:** © 2022 by the authors. Licensee MDPI, Basel, Switzerland. This article is an open access article distributed under the terms and conditions of the Creative Commons Attribution (CC BY) license (<https://creativecommons.org/licenses/by/4.0/>).

## 1. Introduction

Antibiotics have been used extensively in medical, animal husbandry, aquaculture for humans and animal infectious disease treatment [1,2]. Unfortunately, many antibiotics, including fluoroquinolones, sulfonamides, macrolides and tetracycline, have been detected in drinking water, with the concentration ranging from 0.69 to 472.42 ng L<sup>-1</sup>, threatening human health and safety [3–7]. Therefore, it is of great significance to develop drinking water purification for antibiotics removal.

Given the inefficiency of conventional drinking water treatment technologies towards antibiotics [8–10], advanced treatment technologies, such as ozone oxidation [11], activated carbon adsorption [12], advanced oxidation technology [13] and membrane technology [14], have been employed. Due to the favorable separation performance, dispensing with chemicals and continuous operation, membrane technology has attracted considerable attention [15]. Although membrane filtration (such as nanofiltration and reverse osmosis technology) could exclude more than 99% of ciprofloxacin and levofloxacin in treated water [16,17], the application was limited by low flux, high operating pressure and membrane fouling [18].

In the past few years, the electrochemical filtration technology, as an integration of membrane technology with the electrochemical process, has gained popularity for improving treatment performance and mitigating membrane fouling [19]. In an electrochemical filtration process, together with wastewater passing through the membrane electrode, pollutants are adsorbed or intercepted and then electrochemically degraded *in situ*. Compared with the conventional electrochemical process, the intensive convection in flow-through electrochemical filtration remarkably enhances the mass transport and electron transfer of the target substance to the electrode surface, further promoting the removal efficiency [20,21]. Zheng et al. [22] demonstrated that the mass transfer rate of the  $\text{TiO}_2@\text{SnO}_2\text{-Sb}$  electrochemical filtration system in flow-through mode was 3.4 to 5.1 times higher than that in batch mode, and the removal rate of *p*-chloroaniline was increased by 1.4 times. Preferable performance in the removal of antibiotics of electrochemical filtration was also observed. At an operating voltage of 2.5 V and a flow rate of  $1.5 \text{ mL min}^{-1}$ , a carbon nanotubes (CNTs) electrochemical filter achieved a removal rate of more than 98% for tetracycline (TC) [21]. Under the condition of a voltage of 2.03 V and membrane flux of  $300 \text{ L m}^{-2} \text{ h}^{-1}$  (LMH), 95.7% of the sulfanilamide was eliminated by a titanium suboxide ( $\text{Ti}_4\text{O}_7$ ) electrochemical membrane [23]. Although electrochemical filtration has presented its feasibility in removing antibiotics, it is necessary to further improve efficiency and reduce energy consumption, which rely on the performance of the membrane electrode.

Currently, the typical membrane electrodes applied in electrochemical filtration include the CNTs membrane [24,25],  $\text{Ti}_4\text{O}_7$  membrane [26,27] and porous titanium-based membrane [28,29]. Despite the remarkable removal performance, their scale-up applications are hindered by complex preparation processes, high cost and limited flux [30–32]. A polyacrylonitrile (PAN)-based carbon nanofiber membrane prepared by electrospinning, stabilization and carbonization may offer a solution. An electrospun carbon nanofiber membrane (ECNFM) possessing a simple preparation method, low cost, excellent conductivity and high permeate flux is a promising electrochemical membrane [33–35]. Yu et al. [33] prepared PAN-based graphene/tin dioxide carbon nanofibers with a removal efficiency of 85% towards sulfamethoxazole. However, the existing studies focus mostly on the removal performance while neglecting the enhancement of mechanical strength, which is indispensable to supported membrane electrodes. The introduction of terephthalic acid (PTA) into PAN is a feasible approach to enhance the flexibility of carbon nanofibers because the holes generated by PTA sublimation can relieve the stresses on the fibers when bent [36].

In this work, ECNFM using PAN and PTA as precursors was fabricated by electrospinning, stabilization and carbonization, and employed in electrochemical filtration for efficient and economical removal of antibiotic TC. The morphology, structure, mechanical and electrochemical properties of ECNFM were characterized. The effects of the parameters on TC degradation and the long-term operation performance were investigated. Additionally, the efficiency as well as energy demand of TC removal in flow-through and batch mode were compared. The electrochemical oxidation mechanism was explored, and the possible degradation pathways of TC were also proposed according to the high-performance liquid chromatography-tandem mass spectrometry (HPLC-MS-MS). Finally, a safety evaluation of ECNFM-based electrochemical filtration was conducted via the TEST program.

## 2. Materials and Methods

### 2.1. Materials and Reagents

Materials and reagents used in this work are provided in Supplementary Materials (SM) Text S1.

### 2.2. Preparation of ECNFM

The electrospinning method of nanofibers was based on the previous work [37]. Firstly, 4.8 g PAN and 1.6 g PTA were dissolved in 60 mL N, N-Dimethylformamide (DMF) and magnetically stirred for 4 h at  $70 \text{ }^\circ\text{C}$  to prepare the spinning solution. The solution was

then transferred to a movable tank and the electrospinning process was conducted with Nanospider™ NS Lab 2G unit (Elmarco, Liberec, Czech Republic). The conditions of electrospinning are as follows: voltage 60 kV, distance of electrodes 200 mm, moving speed of tank  $100 \text{ mm s}^{-1}$ , temperature  $25 \pm 1 \text{ }^\circ\text{C}$  and humidity  $30 \pm 10\%$ . After electrospinning, the obtained nanofibers were stabilized in air from room temperature to  $270 \text{ }^\circ\text{C}$  at the rate of  $1 \text{ }^\circ\text{C min}^{-1}$ , and then kept for 1 h. Subsequently, the stabilized nanofibers were carbonized at  $1000 \text{ }^\circ\text{C}$  with the heating rate of  $2 \text{ }^\circ\text{C min}^{-1}$  in  $\text{N}_2$  for 2 h to acquire ECNFM. Ultimately, the obtained ECNFM were washed with absolute ethyl alcohol (EtOH) and deionized water (DI water) and dried for further experiments. ECNFM with different PTA weight ratios (0, 1, 2.5, 4%) and carbonization temperatures (800, 900, 1000, 1100  $^\circ\text{C}$ ) were denoted as ECNFM-R-T, where R and T represent PTA ratios in the electrospinning solutions and carbonization temperature, respectively.

### 2.3. Characterization

The surface morphology and structure of ECNFM were observed via scanning electron microscope (SEM, Zeiss Merlin, Oberkochen, Germany). The infrared absorption spectra were obtained by Fourier transform infrared (FTIR, Bruker Vertex 70, Billerica, MA, USA). The surface chemical composition was detected by X-ray photoelectron spectroscopy (XPS, Thermo Fisher Scientific K-Alpha, Waltham, MA, USA). The graphitization degree of ECNFM was analyzed by Raman spectroscopy (Raman, HORIBA Jobin Yvon, Paris, France). The mechanical strength was measured using a universal testing machine (Instron 5967, Canton, MA, USA). Porosity and pore size were determined using mercury intrusion porosimetry (MIP, Micromeritics 9500, Atlanta, GA, USA). Electrical resistance was evaluated via electrochemical impedance spectroscopy (EIS, CHI 760E, Chenhua Inc., Shanghai, China).

### 2.4. Electrochemical Filtration Experiment

The electrochemical filtration experiment of TC removal with ECNFM was illustrated in Figure 1. ECNFM with diameter of 5 cm ( $0.03 \pm 0.005 \text{ g}$ ) and stainless steel mesh served as anode and cathode, respectively, which were connected to a DC power supply with titanium sheets. The anode and cathode were separated by insulating silica gel ring with thickness of 6 mm. The effective filtration area and volume of ECNFM-based electrochemical filter were about  $7.07 \text{ cm}^2$  and  $14.8 \text{ cm}^3$ , respectively. The feed solution with TC as the target pollutants and  $\text{Na}_2\text{SO}_4$  as the supporting electrolyte was pumped into this system constantly by a peristaltic pump. The feed solution sequentially passed through anode and cathode, and the permeate solution was collected at outlet end. All the experiments were performed in triplicate with mean and standard error as results.

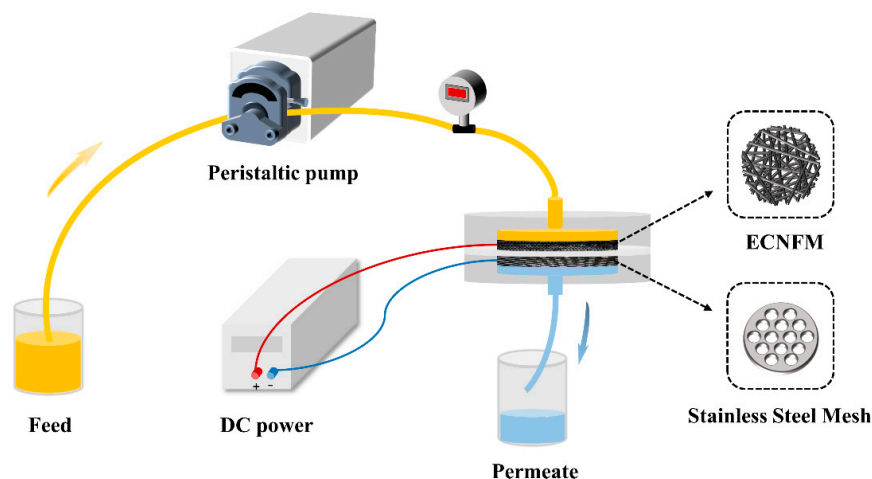


Figure 1. Scheme of ECNFM-based electrochemical filtration.

### 2.5. Analytical Methods

To avoid the photodegradation of TC, TC stock solution and samples were preserved in the brown reagent bottle at 4 °C for further analysis. Samples were filtered through 0.22 µm glass fiber prior to determination of TC concentration via high performance liquid chromatography (HPLC, Waters 2695). The total organic carbon (TOC) was measured using TOC analyzer (Elementar, Langenselbold, Germany). Samples were taken from permeate solution at different hydraulic residence time (0.99, 1.35, 1.64, 2.11, 2.96 min) to detect degradation intermediates by HPLC-MS-MS (Q Exactive Plus). Based on quantitative structure–activity relationship (QSAR) model, the safety of TC and degradation products were evaluated via TEST software.

The removal rate of TC ( $R_{TC}$ ) was calculated by Equation (1):

$$R_{TC} = \left(1 - \frac{C_P}{C_F}\right) \times 100\% \quad (1)$$

where  $C_F$  and  $C_P$  are the TC concentration (ppm) in feed and permeate samples, respectively.

The membrane flux ( $J$ , LMH) of ECNFM-based electrochemical filter was calculated by Equation (2):

$$J = \frac{Q}{A_m} \quad (2)$$

where  $Q$  is the flow rate ( $L h^{-1}$ ) and  $A_m$  is the effective filtration area ( $m^2$ ).

The energy consumption ( $E_C$ ,  $kWh m^{-3}$ ) could be calculated using Equation (3):

$$E_C = \frac{UIt}{V \log\left(\frac{C_F}{C_P}\right)} \quad (3)$$

In particular, for the flow-through electrochemical filtration process,  $E_C$  could be calculated using the following equation:

$$E_C = \frac{UI}{Q \log\left(\frac{C_F}{C_P}\right)} \quad (4)$$

where  $U$ ,  $I$ ,  $t$  and  $V$  are the operating voltage (V), the current intensity (A), the hydraulic retention time (h) and the permeated volume (L), respectively.

## 3. Results and Discussion

### 3.1. Structure, Morphology and Electrochemical Characteristics of ECNFM

The morphologies of electrospun and carbonized nanofibers were observed via SEM. As can be seen from Figure 2a, the electrospun nanofibers owned uniform diameters without obvious beads, and the rough surfaces resulted from solvent evaporation [38]. The carbonized nanofibers maintained stable structures without breaking or collapsing, and they interconnected with each other, which was beneficial to electron transfer (Figure 2b). The diameters of the electrospun and carbonized nanofibers were mainly in the range of 300 to 450 nm (Figure S1), and the average diameter of the nanofibers was slightly decreased from 392 nm to 373 nm after carbonization, which might due to thermal contraction [39]. As shown in Figure S2, the electrospun and carbonized nanofiber membranes were composed of interwoven nanofibers and owned loose porous structures. Moreover, there were some pores inside the carbon nanofiber matrix resulted from PTA sublimation, which was beneficial to improve the tensile strength and porosity.

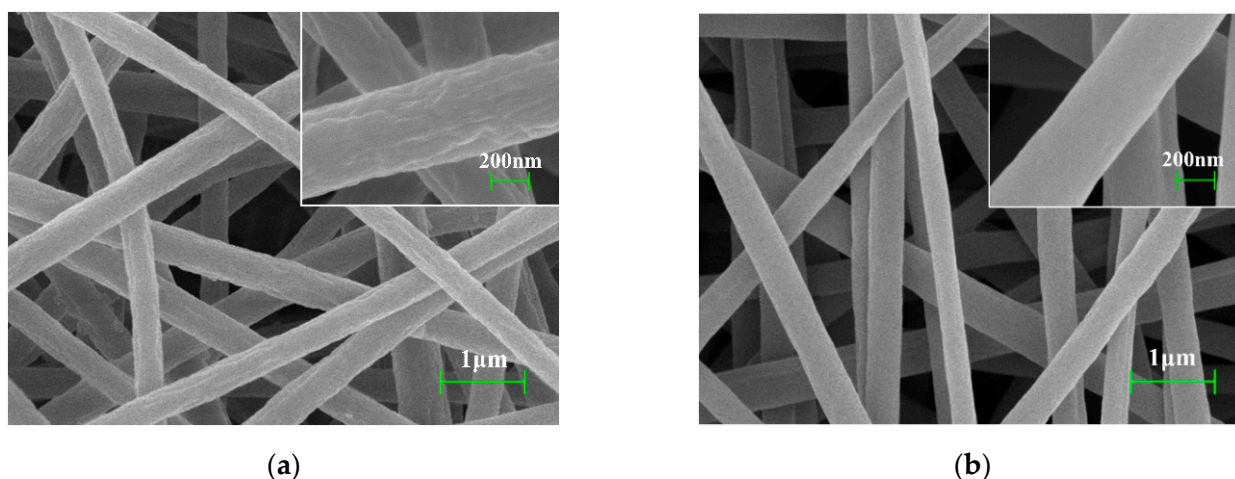


**Figure 2.** SEM images of (a) electrospun nanofibers (2.5 wt% PTA) and (b) carbonized nanofibers (ECNFM-2.5%-1000).

The effect of PTA on the tensile stress of ECNFM was explored, as shown in Figure 3a. With the PTA weight ratios increasing from 0 to 2.5%, the tensile stress was significantly enhanced from 0.12 to 0.75 MPa, indicating that adding PTA promoted the mechanical strength of ECNFM. However, only a slight increase (0.1 MPa) in the tensile stress of ECNFM-4%-1000 was observed, which might be due to the limited solubility of PTA in spinning solution. The flexibility before and after the addition of PTA was also compared by bending and twisting (Figure S3). Different from the cracked ECNFM-0-1000 after bending, ECNFM-2.5%-1000 could be bent and twisted easily, exhibiting the potential as a membrane electrode. The improvement on mechanical strength might be attributed to the sublimation of PTA, which created holes on the nanofibers to relieve stress [36].

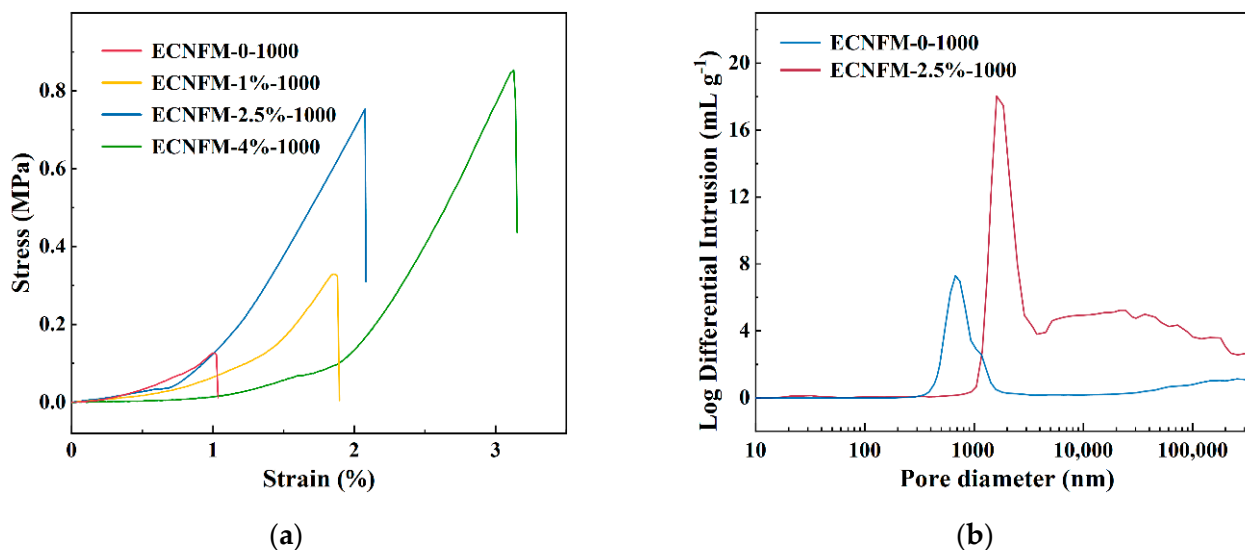


**Figure 3.** (a) Tensile stress–strain curves of ECNFM-R-1000 (R = 0, 1, 2.5, 4%); (b) pore distribution of ECNFM-R-1000 (R = 0, 2.5%).

The pore structures of ECNFM-R-1000 (R = 0, 2.5%) were further investigated by MIP. It was found that ECNFM-0-1000 and ECNFM-2.5%-1000 were macroporous structures with average pore sizes of 1.07 and 2.52  $\mu\text{m}$  (Figure 3b), and the porosity was 80.0% and 92.8%, respectively (Table S1). Furthermore, the permeation fluxes of ECNFM-0-1000 and ECNFM-2.5%-1000 were measured to be  $7.66 \times 10^4 \text{ L m}^{-2} \text{ h}^{-1} \text{ bar}^{-1}$  and  $1.15 \times 10^5 \text{ L m}^{-2}$

$\text{h}^{-1} \text{bar}^{-1}$ , respectively. These results demonstrated that the sublimation of PTA could increase the porosity of ECNFM, which was conducive to improving permeation flux and enhancing convection [40,41].

FTIR technology was employed to explore the bond structure of nanofibers synthesized at different stages, as shown in Figure 4a. In the FTIR curve of the electrospun membrane, the characteristic peaks at 1231, 1298, 1690 and 2243  $\text{cm}^{-1}$  belonged to C-O, C-OH, C=O and C $\equiv$ N functional groups of the precursors of PAN and PTA [42,43]. After stabilization, the peak corresponding to C $\equiv$ N groups vanished, whereas a sharp peak appeared at 1585  $\text{cm}^{-1}$  related to the C=N and C=C functional groups [43]. The variation in functional groups indicated the occurrence of dehydrogenation and cyclization of C $\equiv$ N to form a heat-resistant ladder structure, which could maintain the structural stability of nanofibers in the carbonization process [44]. As can be seen from Figure S4, the color of the stabilized fibers turned to yellow, verifying the formation of chromogenic groups, such as C=C and C=N [45]. In the FTIR curve of ECNFM, the intensity of above adsorption peaks was decreased and new characteristic bands of C-C at 1567  $\text{cm}^{-1}$  and C=C at 1140  $\text{cm}^{-1}$  appeared, which were attributed to dehydrogenation, denitrification and generation of the aromatic ring structure [46]. With the carbonization temperature rising to 1000  $^{\circ}\text{C}$ , the FTIR spectrum became flat and the characteristic peaks almost disappeared, implying the completion of the carbonization process, during which a graphite-like structure was formed [46].

XPS technology was used to further reveal the elemental composition and bond structure of ECNFM-2.5%-1000. The survey spectra displayed three typical peaks corresponding to the elements of C, N and O. The doped N, which is beneficial to promote conductivity of ECNMF, derived from the decomposition of PAN and  $\text{N}_2$  introduced in the carbonization process (Figure 4b inset) [47]. The O atoms might come from introduced  $\text{O}_2$  in the stabilization process and precipitated PTA on the surface. Meanwhile, the C 1s spectrum could be divided into three individual peaks located at 284.87, 286.02 and 288.69 eV related to C-C, C-O or C-N and C=O, respectively, and C-C bonds possessed the highest relative abundance among them (Figure 4b) [48]. In summary, the precursors of PAN and PTA have been converted into carbon materials successfully after stabilization and carbonization at 1000  $^{\circ}\text{C}$  based on the results of FTIR and XPS.

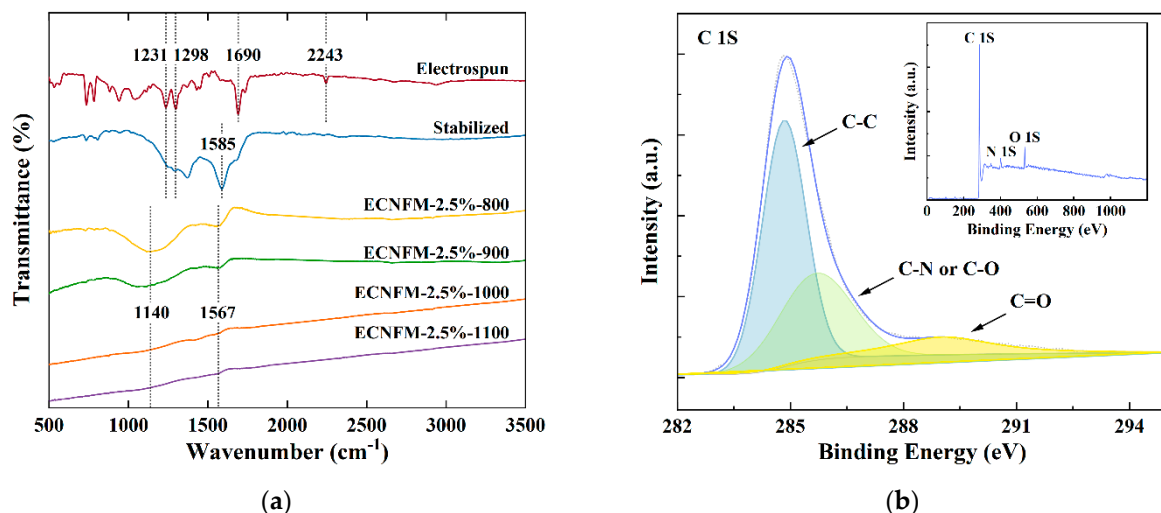


**Figure 4.** (a) FTIR spectra of ECNFM-2.5%-T (T = 800, 900, 1000, 1100  $^{\circ}\text{C}$ ); (b) high-resolution of C 1s spectrum (inset panel: full survey scan) of ECNFM-2.5%-1000.

Raman technology was employed to explore the carbon structure of the ECNFM at different carbonization temperatures (Figure 5a). Generally, the degree of graphitization of the carbon nanofibers can be measured by the intensity ratio of the D and G bands ( $I_D/I_G$ ), which are located at 1350 and 1580  $\text{cm}^{-1}$  in the spectrum, respectively, and the smaller  $I_D/I_G$  value suggests the higher degree of graphitization and regularity of the carbon structure, as well as enhanced electrical conductivity [49]. The  $I_D/I_G$  values of ECNFM carbonized at 800, 900, 1000 and 1100  $^{\circ}\text{C}$  were calculated as 1.12, 1.00, 0.97 and 0.96, respectively, implying that the increase in carbonization temperature would facilitate the graphitization and electrical conductivity of ECNFM.

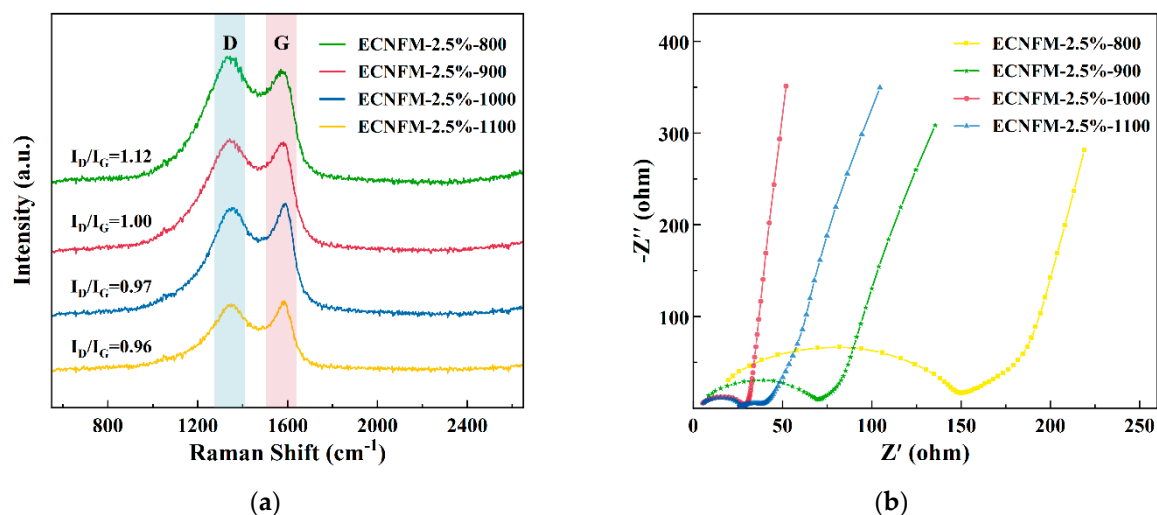


**Figure 5.** (a) Raman spectra and (b) EIS plot of ECNFM-2.5%-T (T = 800, 900, 1000, 1100  $^{\circ}\text{C}$ ).

The electrical conductivity of ECNFM was further confirmed via EIS measurements, as shown in Figure 5b. The diameter of semicircles in the high frequency region represents the electron transfer resistance ( $R_{ct}$ ) [37]. With the carbonization temperature increasing from 800 to 1000  $^{\circ}\text{C}$ , the value of  $R_{ct}$  decreased notably from 130.23 to 23.52  $\Omega$ , and then came to 21.82  $\Omega$  at 1100  $^{\circ}\text{C}$ , which was in agreement with the Raman analyses. These results confirmed that the conductivity of ECNFM could be promoted by carbonization, which was mostly completed above 1000  $^{\circ}\text{C}$ .

Considering performance and energy consumption comprehensively, ECNFM-2.5%-1000 was chosen for subsequent experiments.

### 3.2. Effect of Operational Parameters on TC Removal during Electrochemical Filtration

Under the condition of pH 6.1,  $\text{Na}_2\text{SO}_4$  0.1  $\text{mol L}^{-1}$ , TC 10 ppm, membrane flux 594 LMH, the effect of the applied voltage on TC removal by ECNFM-based electrochemical filtration was depicted in Figure 6a. The TC removal rate was lower than 5% when the voltage was 0–1 V. With the voltage further improving, a sharply enhanced TC removal rate was observed and reached the maximum at 2 V (99.1%), which dropped to 86.0% at 4 V. The low TC removal rate (1.2%) without the assistance of applied voltage suggested a poor adsorption performance of ECNFM-2.5%-1000. However, with an excessive voltage, the bubbles produced by the side reaction of oxygen evolution would hinder the contact between the TC molecules and ECNFM-2.5%-1000, working against TC removal. Thus, 2 V was chosen as the optimal operating voltage for follow-up studies.

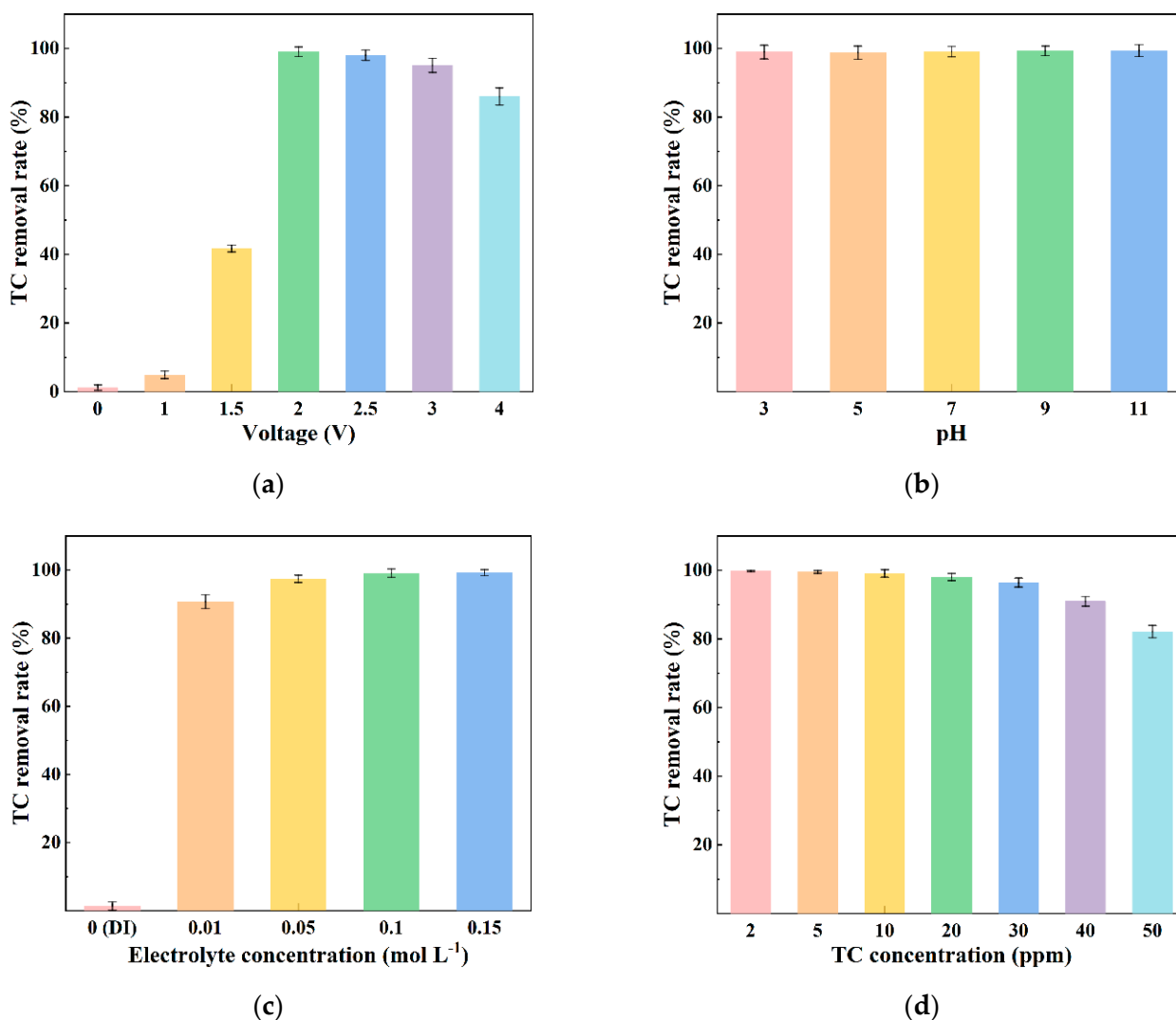


**Figure 6.** Effects of (a) applied voltage, (b) pH, (c) electrolyte concentration and (d) initial TC concentration on TC removal rate in ECNFM-based electrochemical filter. The volume of treated water was 250 mL.

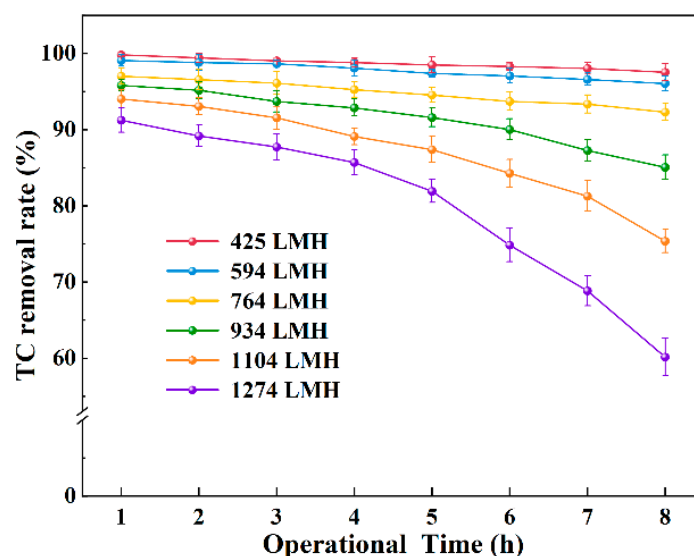
The pH value of the feed was adjusted using 0.1 mol L<sup>-1</sup> H<sub>2</sub>SO<sub>4</sub> or NaOH to explore the effect of pH. As shown in Figure 6b, the TC removal rate was maintained above 99% in the pH range of 3 to 11, which was different from most of the previous reports that the electrochemical treatment performance is greatly influenced by the pH condition due to the pH-dependent generation of •OH [50]. The possible reason was the nonparticipation of •OH in TC removal. A similar phenomenon was also observed in TC removal by Ti/RuO<sub>2</sub>-IrO<sub>2</sub> anode [51]. The natural pH of 6.1 without adjustment was selected for subsequent experiments.

Figure 6c illustrates the TC removal efficiency as a function of Na<sub>2</sub>SO<sub>4</sub> concentration. The removal rate of TC (<2%) in DI water was equally matched with that without applied voltage. The main reason was that low conductivity was disadvantageous to the electrochemical reaction, further confirming the main role of electrochemical oxidation in the removal of TC. With the Na<sub>2</sub>SO<sub>4</sub> concentration increasing from 0.01 to 0.15 mol L<sup>-1</sup>, the TC removal raised from 90.7% to 99.2% gradually. In the flow-through process, the continuous convection on the membrane electrode surface promotes charge neutralization, reducing the sensitivity to ionic strength [52]. Therefore, a high TC removal rate was achieved in a wide range of electrolyte concentrations (0.01–0.15 mol L<sup>-1</sup>).

The effect of the initial TC concentration on treatment performance by ECNFM-based electrochemical filtration can be seen from Figure 6d. The highest removal rate (99.8%) was obtained when the TC concentration was 2 ppm. The TC removal rate slightly decreased to 96.4% with 30 ppm TC, and then reduced obviously to 82.2% under the condition of 50 ppm TC, which might be due to the limited surface active sites of ECNFM-2.5%-1000. It was confirmed that the electrochemical filtration technology was tailored for the condition of low pollutant concentration, indicating its application potential for drinking water treatment [19].

### 3.3. Long-Term Operation Performance for TC Removal

To test the long-term operational stability of the ECNFM-based electrochemical filter, an 8-h continuous operation experiment was performed in flow-through mode (condition: voltage 2 V, pH 6.1,  $\text{Na}_2\text{SO}_4$  0.1 mol L<sup>-1</sup>, TC 10 ppm), as displayed in Figure 7. In the first hour, the ECNFM-2.5%-1000 reached the highest TC removal rate of 99.8% with the optimal flux of 425 LMH (corresponding flow rate and hydraulic residence time were 5 mL min<sup>-1</sup> and 2.96 min, respectively). The removal rate then decreased gradually with the increase of flux and dropped to 91.2% at 1274 LMH (corresponding flow rate and hydraulic residence time were 15 mL min<sup>-1</sup> and 0.99 min, respectively). This might be due to the short residence time in the filter, resulting in insufficient contact between TC molecules and the active sites of ECNFM [53]. After 8 h of continuous treatment, the TC removal rate decreased marginally from 99.8% to 97.5% at 425 LMH, implying a good treatment stability. It could be verified by no obvious damage to the used ECNFM-2.5%-1000, as shown in Figure S5. Nevertheless, the removal rate remarkably dropped from 91.2% to 60.2% when the flux was 1274 LMH, which might be attributed to the excessed treatment load. All the same, the treatment efficiency of the ECNFM-based electrochemical filter is superior to most of the state-of-the-art electrochemical filtration processes (Table S2), which might be attributed to the high porosity and excellent conductivity of ECNFM-2.5%-1000.



**Figure 7.** 8-h continuous operation performance. Experimental condition: voltage = 2 V, natural pH = 6.1,  $[\text{Na}_2\text{SO}_4] = 0.1 \text{ mol L}^{-1}$ ,  $[\text{TC}] = 10 \text{ ppm}$ .

### 3.4. Comparison of Efficacy and Energy Consumption between Flow-Through and Batch Mode

The efficacies in flow-through and batch mode were compared via kinetics analysis, as illustrated in Figure 8a. The electrochemical degradation of TC by the ECNFM-based electrochemical filter was well-matched with pseudo-first-order kinetics, and the reaction rate constant ( $k$ ) was 2.28 min<sup>-1</sup> in flow-through mode, which was 10.53 times higher than that in batch mode (0.22 min<sup>-1</sup>). In the conventional electrolysis process under batch operation,

the limited contact area leads to the inferior mass transfer rate and lower reaction efficiency, which can be improved by the enhanced convection in flow-through operation [20,21]. The flow-through configuration would be a potential strategy to efficiently improve the treatment performance of the electrochemical process.

Energy consumption (EC) is a key parameter that should be considered for water treatment. Based on 90% TC removal, EC with applied voltages in flow-through and batch modes was calculated (Figure 8b). Benefiting from the high treatment efficiency, the EC values of the flow-through operation were obviously lower than that of the batch operation in all the conditions. The EC of the ECNFM-based electrochemical filter in the flow-through configuration raised from 0.016 to 0.085 kWh m<sup>-3</sup>, with the applied voltage increasing from 1.5 to 3 V and then sharply reaching 0.278 kWh m<sup>-3</sup> at 4 V owing to the occurrence of side reactions, such as oxygen evolution, demonstrating the importance of adjusting applied voltage. Compared with similar studies (Table S2), ECNFM-2.5%-1000 possessed a lower EC, which was closely related to its high permeate flux and electron transport efficiency endowed by the large porosity and low electrical resistance.

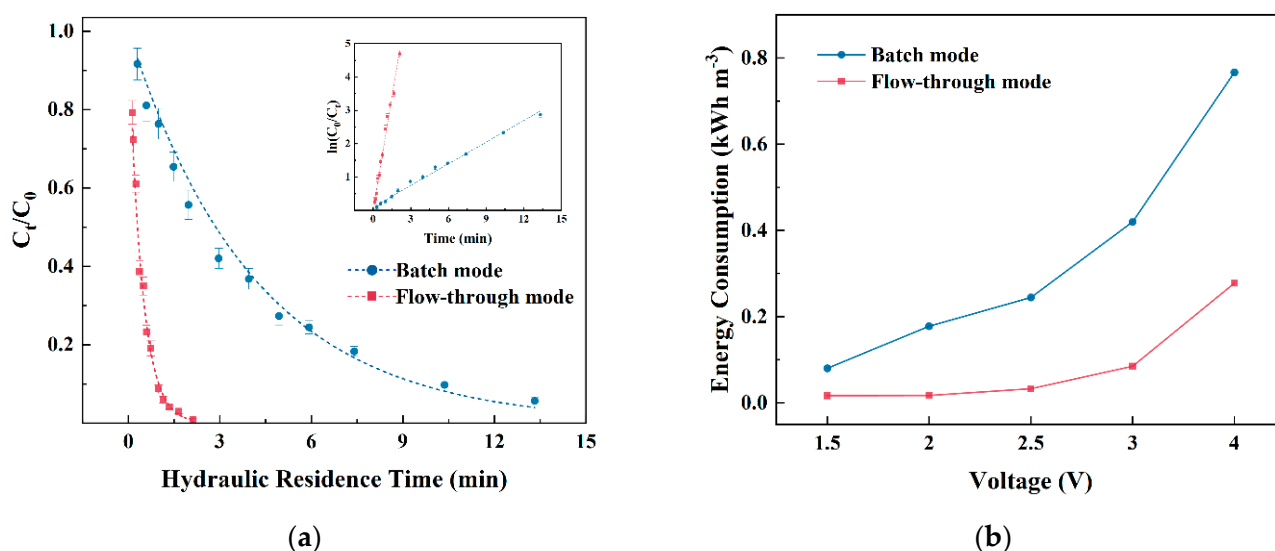


**Figure 8.** (a) Kinetics and (b) energy consumption of TC degradation under batch and flow-through modes.

### 3.5. The Removal Mechanism of TC

#### 3.5.1. Electrochemical Oxidation Mechanism

The electrochemical oxidation pattern involves direct anodic oxidation and indirect anodic oxidation. Cyclic voltammetry (CV), linear sweep voltammetry (LSV), open-circuit potential (OCP) measurements and scavenging experiments were employed to reveal the anodic oxidation mechanism of ECNFM-2.5%-1000. Oxalic acid (OA) was used as the probe to verify the direct oxidation mechanism via CV analysis, which was carried out in 0.1 mol L<sup>-1</sup> Na<sub>2</sub>SO<sub>4</sub> solution. As shown in Figure 9a, a distinct oxidation peak appeared at 0.82 V (vs. Ag/AgCl) on the CV curve with the addition of 10 mmol L<sup>-1</sup> OA, whereas no peak was observed in the absence of OA, implying the existence of a direct oxidation reaction. The higher oxygen evolution potential (OEP) of ECNFM-2.5%-1000 (1.3 V vs. Ag/AgCl) in the LSV curve (Figure S6) further confirmed the theoretical feasibility of direct anodic oxidation [54].

In the path of indirect anodic oxidation, reactive oxygen species participated in the degradation of organics. In an ECNFM-based electrochemical filter using Na<sub>2</sub>SO<sub>4</sub> as an electrolyte, the active oxidation species, such as  $\bullet\text{OH}$  and  $\text{SO}_4^{\bullet-}$ , might be generated and serve as oxidizers. The OCP method was applied to explore the potential distribution of the anode and cathode. As depicted in Figure 9b, the anodic potential was 1 V (vs. Ag/AgCl)

at a total voltage of 2 V, much lower than the thermodynamic potentials for the formation of  $\bullet\text{OH}$  (2.18 V vs. Ag/AgCl) and  $\text{SO}_4^{\bullet-}$  (2.2 V vs. Ag/AgCl) [41]. Whereas, under higher applied voltage, the oxygen evolution reaction of ECNFM-2.5%-1000 possessed a greater preponderance than the production of  $\bullet\text{OH}$  and  $\text{SO}_4^{\bullet-}$  due to the lower OEP (1.3V), inhibiting the generation of  $\bullet\text{OH}$  and  $\text{SO}_4^{\bullet-}$ . Furthermore, Tert-butyl Alcohol (TBA) and EtOH with a concentration of 10 mmol L<sup>-1</sup> were introduced to the feed solution as the scavengers to investigate the action of  $\bullet\text{OH}$  and  $\text{SO}_4^{\bullet-}$ , respectively [32]. As expected, the removal rate of TC displayed negligible change in the presence of scavengers (Figure S7), which agreed with the results of the OCP analysis.

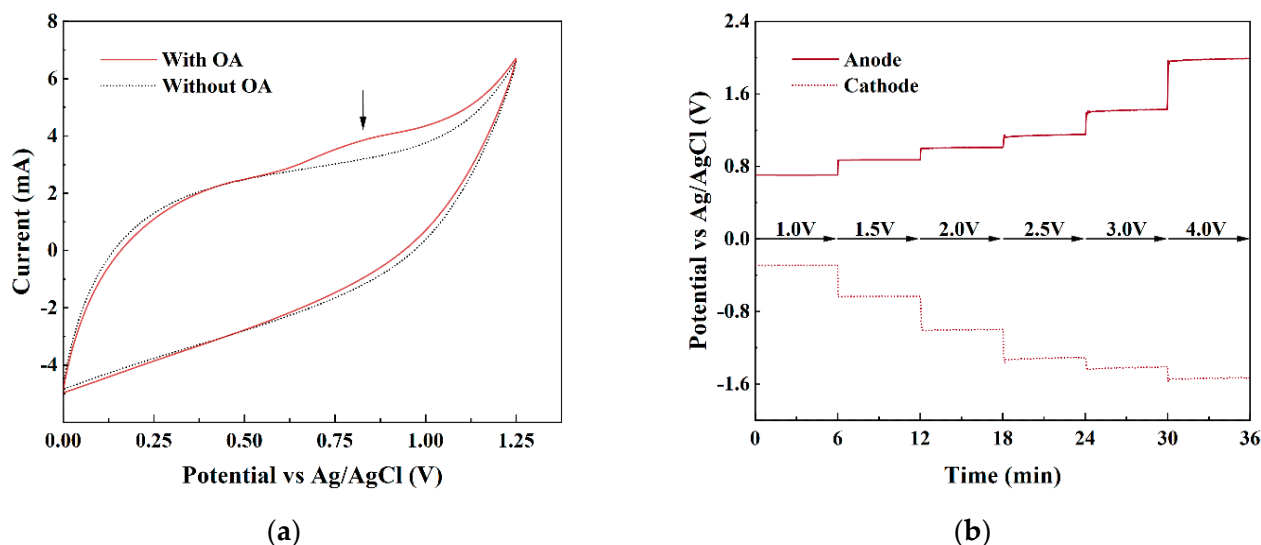


**Figure 9.** (a) CV curves of ECNFM-2.5%-1000 with or without OA; (b) anode and cathode potential as a function of applied voltage.

Accordingly, the direct anodic oxidation instead of indirect oxidation accounted for TC degradation due to the low OEP and anode potential of ECNFM-2.5%-1000. Direct oxidation is usually thought to be inefficient because of mass transfer limitations, which can be overcome by the enhanced convection in the flow-through configuration of an ECNFM-based electrochemical filter.

### 3.5.2. Proposed TC Degradation Pathway and Safety Evaluation

The intermediate products of TC were detected via HPLC-MS-MS analysis, including six compounds with  $m/z = 401, 381, 308, 224, 166$  and  $122$ , as listed in Table S3 and Figure S8. The degradation pathway of TC in the ECNFM-based electrochemical filter was proposed and shown in Figure 10. The parent compound TC underwent the deamidation processes to form product A ( $m/z = 401$ ). After that, product A was converted to product B ( $m/z = 381$ ) by cleaving the carbon–carbon double bond and losing methyl group, or product C ( $m/z = 308$ ), via deamination and demethylation. Product C was further transformed into product D ( $m/z = 224$ ) via the ring-opening process. With the occurrence of ring opening and dehydroxylation, product D was degraded to product E ( $m/z = 166$ ), which was demethylated to product F ( $m/z = 122$ ) and other small molecules eventually. In conclusion, the electrochemical degradation of TC mainly involved the removal of functional groups and ring-opening reaction, which was consistent with previous findings [55].

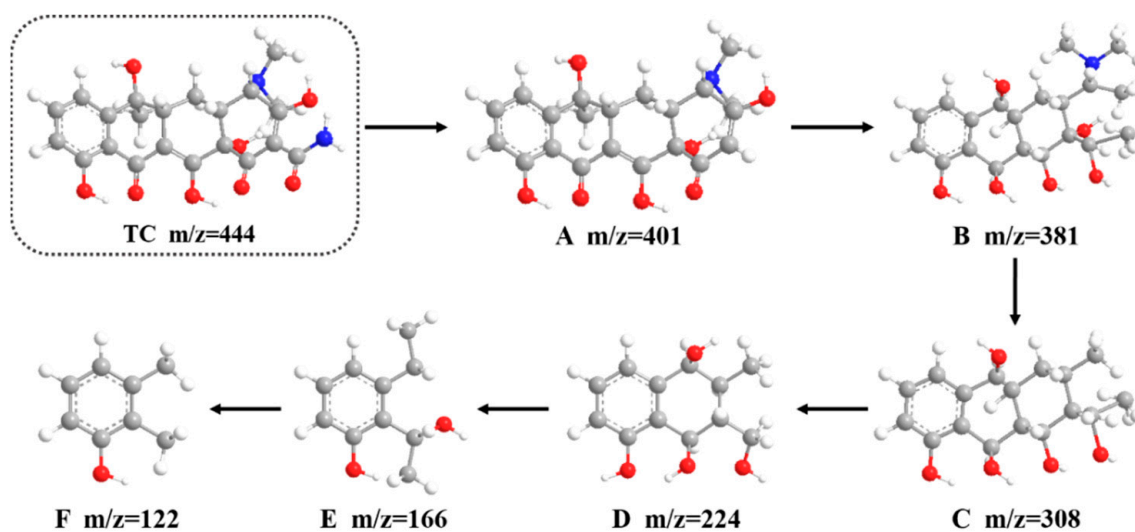


Figure 10. Proposed degradation pathway of TC.

Based on the QSAR model, the developmental toxicity and mutagenicity of TC and degradation products were estimated via TEST software. As displayed in Figure 11a, the developmental toxicity values of all the intermediates were lower than TC. Products A, B and C remained mutagenicity positive, while products D, E and F were supposed to be mutagenicity negative (Figure 11b). The remaining toxicity in the treated water might be ascribed to the incomplete degradation of TC, which was in accordance with the results of the TOC analysis (Figure S9).

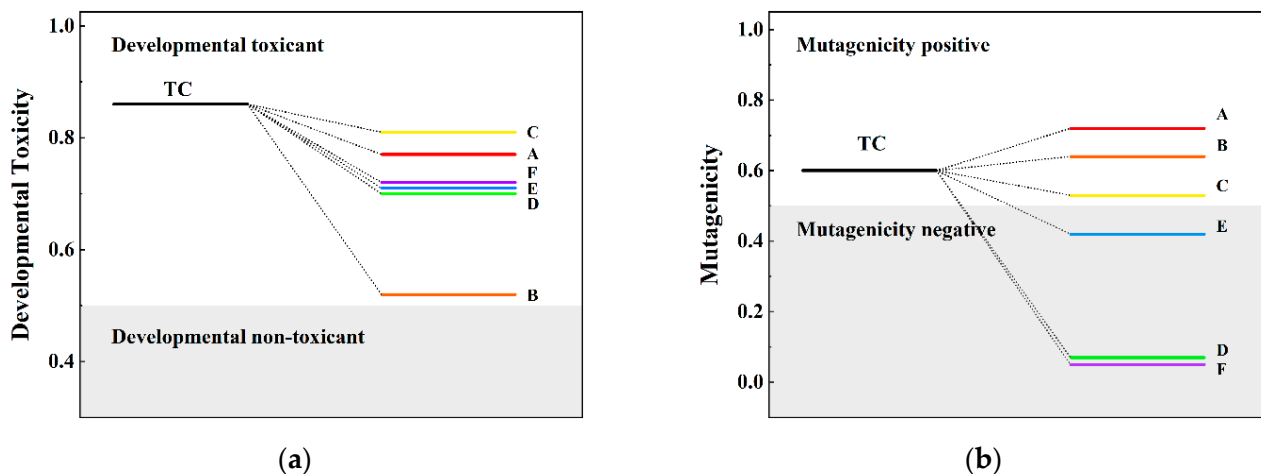


Figure 11. (a) Developmental toxicity and (b) mutagenicity of TC and the intermediates.

### 3.5.3. Removal Mechanism of TC by ECNFM-Based Electrochemical Filter

The removal mechanism of TC in an ECNFM-based electrochemical filter was put forward. Under the flow-through mode, when the feed passes through the membrane anode with high porosity, the enhanced convection contributed to the rapider mass transfer of TC molecules with ECNFM-2.5%-1000. Meanwhile, the TC molecules were degraded immediately efficiently in situ to intermediates with lower toxicity, in which the oxygen evolution reaction was avoided and the corresponding energy consumption decreased. When the TC removal rate reached 99.1%, the energy consumption was as low as  $0.017 \text{ kWh m}^{-3}$ , making ECNFM-based electrochemical filtration an efficient and low-cost technology.

#### 4. Conclusions

This work suggested an efficient and economical approach for TC removal by an electrochemical filter based on an ECNFM-2.5%-1000 anode. The mechanical strength and porosity of ECNFM-2.5%-1000 were improved by the addition of PTA, and the electron transfer conductivity was increased after high-temperature carbonization. A superior TC removal efficiency of 99.8% was gained under a high flux of 425 LMH. By virtue of the high porosity and conductivity of ECNFM-2.5%-1000, the enhanced TC removal rate ( $2.28 \text{ min}^{-1}$ ) and the decreased energy consumption ( $0.017 \text{ kWh m}^{-3}$ ) were observed in flow-through mode. According to the product analysis, TC could be converted to intermediates with lower toxicity via the loss of functional groups and ring opening reaction, which was mainly achieved by the direct anodic oxidation. Overall, ECNFM-based electrochemical filtration was demonstrated as a promising drinking water purification. Nevertheless, how to introduce indirect anodic oxidation via optimizing ECNFM-2.5%-1000 to facilitate the mineralization of TC needs to be further investigated, which is of great significance to ensure the safety of this process.

**Supplementary Materials:** The following supporting information can be downloaded at: <https://www.mdpi.com/article/10.3390/w14060910/s1>. Text S1: Materials and reagents; Figure S1. Histograms of nanofiber diameter of (a) electrospun nanofibers (2.5 wt% PTA) and (b) carbonized nanofibers (ECNFM-2.5%-1000). Figure S2. Cross-sectional images of (a) electrospun nanofibers (2.5 wt% PTA) and (b) carbonized nanofibers (ECNFM-2.5%-1000). Figure S3: Photographs of (a) ECNFM and (b) ECNFM-2.5%-1000; Figure S4: Photographs of (a) electrospun, (b) stabilized, (c) carbonized nanofiber membrane; Figure S5: SEM images of ECNFM-2.5%-1000 after 8-h continuous operation; Figure S6: Linear sweep voltammetry (LSV) curve; Figure S7: Effect of scavengers on TC removal rate; Figure S8: Secondary MS spectra of TC and the possible identified intermediates; Figure S9: TOC measurement as a function of permeate flux; Table S1: Characteristics of ECNFM; Table S2: Performance comparison of ECNFM-based electrochemical filter with other electrochemical filtration system; Table S3: The information of the possible intermediates products.

**Author Contributions:** X.Y.: Investigation, Methodology, Software, Formal analysis, Writing—Original Draft; X.L.: Validation, Writing—Review and Editing; Y.H.: Conceptualization, Writing—Review and Editing, Supervision, Funding acquisition; J.C.: Funding acquisition; Y.C.: Funding acquisition. All authors have read and agreed to the published version of the manuscript.

**Funding:** This research received no external funding.

**Institutional Review Board Statement:** Not applicable.

**Informed Consent Statement:** Not applicable.

**Data Availability Statement:** Not applicable.

**Acknowledgments:** We sincerely thank Yating Jia, Chun Xiao and Yueyue Shi for writing assistance.

**Conflicts of Interest:** The authors declare no conflict of interest.

#### References

1. Kovaláková, P.; Cizmas, L.; McDonald, T.J.; Marsalek, B.; Feng, M.; Sharma, V.K. Occurrence and toxicity of antibiotics in the aquatic environment: A review. *Chemosphere* **2020**, *251*, 126351. [[CrossRef](#)] [[PubMed](#)]
2. Wang, J.; Zhuan, R. Degradation of antibiotics by advanced oxidation processes: An overview. *Sci. Total Environ.* **2020**, *701*, 135023. [[CrossRef](#)] [[PubMed](#)]
3. Liu, Y.; Chen, Y.; Feng, M.; Chen, J.; Shen, W.; Zhang, S. Occurrence of antibiotics and antibiotic resistance genes and their correlations in river-type drinking water source, China. *Environ. Sci. Pollut. Res.* **2021**, *28*, 42339–42352. [[CrossRef](#)] [[PubMed](#)]
4. He, P.; Wu, J.; Peng, J.; Wei, L.; Zhang, L.; Zhou, Q.; Wu, Z. Pharmaceuticals in drinking water sources and tap water in a city in the middle reaches of the Yangtze River: Occurrence, spatiotemporal distribution, and risk assessment. *Environ. Sci. Pollut. Res.* **2021**, *29*, 2365–2374. [[CrossRef](#)] [[PubMed](#)]
5. Benotti, M.J.; Trenholm, R.A.; Vanderford, B.J.; Holady, J.C.; Stanford, B.D.; Snyder, S. Pharmaceuticals and endocrine disrupting compounds in US drinking water. *Environ. Sci. Technol.* **2009**, *43*, 597–603. [[CrossRef](#)] [[PubMed](#)]

6. Padhye, L.; Yao, H.; Kung'U, F.T.; Huang, C.-H. Year-long evaluation on the occurrence and fate of pharmaceuticals, personal care products, and endocrine disrupting chemicals in an urban drinking water treatment plant. *Water Res.* **2014**, *51*, 266–276. [[CrossRef](#)]
7. Reichert, G.; Hilgert, S.; Fuchs, S.; Azevedo, J.C.R. Emerging contaminants and antibiotic resistance in the different environmental matrices of Latin America. *Environ. Pollut.* **2019**, *255*, 113140. [[CrossRef](#)] [[PubMed](#)]
8. Watkinson, A.; Murby, E.; Costanzo, S. Removal of antibiotics in conventional and advanced wastewater treatment: Implications for environmental discharge and wastewater recycling. *Water Res.* **2007**, *41*, 4164–4176. [[CrossRef](#)] [[PubMed](#)]
9. Vieno, N.M.; Härkki, H.; Tuhkanen, T.; Kronberg, L. Occurrence of pharmaceuticals in river water and their elimination in a pilot-scale drinking water treatment plant. *Environ. Sci. Technol.* **2007**, *41*, 5077–5084. [[CrossRef](#)] [[PubMed](#)]
10. Vieno, N.; Tuhkanen, T.; Kronberg, L. Removal of pharmaceuticals in drinking water treatment: Effect of chemical coagulation. *Environ. Technol.* **2006**, *27*, 183–192. [[CrossRef](#)] [[PubMed](#)]
11. Liu, J.; Sun, Q.; Zhang, C.; Li, H.; Song, W.; Zhang, N.; Jia, X. Removal of typical antibiotics in the advanced treatment process of productive drinking water. *Desalin. Water Treat.* **2016**, *57*, 11386–11391. [[CrossRef](#)]
12. Xiang, Y.; Xu, Z.; Wei, Y.; Zhou, Y.; Yang, X.; Yang, Y.; Yang, J.; Zhang, J.; Luo, L.; Zhou, Z. Carbon-based materials as adsorbent for antibiotics removal: Mechanisms and influencing factors. *J. Environ. Manag.* **2019**, *237*, 128–138. [[CrossRef](#)] [[PubMed](#)]
13. Xiao, C.; Li, X.; Li, Q.; Hu, Y.; Cheng, J.; Chen, Y. Ni-doped FeC<sub>2</sub>O<sub>4</sub> for efficient photo-Fenton simultaneous degradation of organic pollutants and reduction of Cr(VI): Accelerated Fe(III)/Fe(II) cycle, enhanced stability and mechanism insight. *J. Clean. Prod.* **2022**, *340*, 130775. [[CrossRef](#)]
14. Yang, G.; Zhang, D.; Wang, C.; Liu, H.; Qu, L.; Li, H. A novel nanocomposite membrane combining BN nanosheets and GO for effective removal of antibiotic in water. *Nanomaterials* **2019**, *9*, 386. [[CrossRef](#)]
15. Huang, A.; Yan, M.; Lin, J.; Xu, L.; Gong, H.; Gong, H. A review of processes for removing antibiotics from breeding wastewater. *Int. J. Environ. Res. Public Health* **2021**, *18*, 4909. [[CrossRef](#)] [[PubMed](#)]
16. Cristóvão, M.B.; Tela, S.; Silva, A.F.; Oliveira, M.; Bento-Silva, A.; Bronze, M.R.; Crespo, M.T.B.; Crespo, J.G.; Nunes, M.; Pereira, V.J. Occurrence of antibiotics, antibiotic resistance genes and viral genomes in wastewater effluents and their treatment by a pilot scale nanofiltration unit. *Membranes* **2021**, *11*, 9. [[CrossRef](#)] [[PubMed](#)]
17. Alonso, J.J.S.; El Kori, N.; Melián-Martel, N.; Del Río-Gamero, B. Removal of ciprofloxacin from seawater by reverse osmosis. *J. Environ. Manag.* **2018**, *217*, 337–345. [[CrossRef](#)] [[PubMed](#)]
18. Pan, Z.; Yu, F.; Li, L.; Song, C.; Yang, J.; Wang, C.; Pan, Y.; Wang, T. Electrochemical microfiltration treatment of bisphenol A wastewater using coal-based carbon membrane. *Sep. Purif. Technol.* **2019**, *227*, 115695. [[CrossRef](#)]
19. Li, C.; Zhang, M.; Song, C.; Tao, P.; Sun, M.; Shao, M.; Wang, T. Enhanced treatment ability of membrane technology by integrating an electric field for dye wastewater treatment: A review. *J. AOAC Int.* **2018**, *101*, 1341–1352. [[CrossRef](#)]
20. Li, Z.; Shen, C.; Liu, Y.; Ma, C.; Li, F.; Yang, B.; Huang, M.; Wang, Z.; Dong, L.; Wolfgang, S. Carbon nanotube filter functionalized with iron oxychloride for flow-through electro-Fenton. *Appl. Catal. B Environ.* **2020**, *260*, 118204. [[CrossRef](#)]
21. Liu, Y.; Liu, H.; Zhou, Z.; Wang, T.; Ong, C.N.; Vecitis, C.D. Degradation of the common aqueous antibiotic tetracycline using a carbon nanotube electrochemical filter. *Environ. Sci. Technol.* **2015**, *49*, 7974–7980. [[CrossRef](#)] [[PubMed](#)]
22. Zheng, J.; Wang, Z.; Ma, J.; Xu, S.; Wu, Z. Development of an electrochemical ceramic membrane filtration system for efficient contaminant removal from waters. *Environ. Sci. Technol.* **2018**, *52*, 4117–4126. [[CrossRef](#)]
23. Misal, S.N.; Lin, M.-H.; Mehraeen, S.; Chaplin, B.P. Modeling electrochemical oxidation and reduction of sulfamethoxazole using electrocatalytic reactive electrochemical membranes. *J. Hazard. Mater.* **2020**, *384*, 121420. [[CrossRef](#)]
24. Cunha, G.D.S.; de Souza-Chaves, B.M.; Bila, D.; Bassin, J.; Vecitis, C.D.; Dezotti, M. Insights into estrogenic activity removal using carbon nanotube electrochemical filter. *Sci. Total Environ.* **2019**, *678*, 448–456. [[CrossRef](#)] [[PubMed](#)]
25. Zhao, L.; Zhang, X.; Liu, Z.; Deng, C.; Xu, H.; Wang, Y.; Zhu, M. Carbon nanotube-based electrocatalytic filtration membrane for continuous degradation of flow-through Bisphenol A. *Sep. Purif. Technol.* **2021**, *265*, 118503. [[CrossRef](#)]
26. Trellu, C.; Coetsier, C.; Rouch, J.-C.; Esmilaire, R.; Rivallin, M.; Cretin, M.; Causserand, C. Mineralization of organic pollutants by anodic oxidation using reactive electrochemical membrane synthesized from carbothermal reduction of TiO<sub>2</sub>. *Water Res.* **2018**, *131*, 310–319. [[CrossRef](#)] [[PubMed](#)]
27. Liu, Y.; Mei, J.; Shen, C.; Huang, M.; Yang, M.; Wang, Z.; Sand, W.; Li, F. Rapid and selective electrochemical transformation of ammonia to N<sub>2</sub> by substoichiometric TiO<sub>2</sub>-based electrochemical system. *RSC Adv.* **2020**, *10*, 1219–1225. [[CrossRef](#)]
28. Li, D.; Tang, J.; Zhou, X.; Li, J.; Sun, X.; Shen, J.; Wang, L.; Han, W. Electrochemical degradation of pyridine by Ti/SnO<sub>2</sub>-Sb tubular porous electrode. *Chemosphere* **2016**, *149*, 49–56. [[CrossRef](#)]
29. Yang, K.; Lin, H.; Liang, S.; Xie, R.; Lv, S.; Niu, J.; Chen, J.; Hu, Y. A reactive electrochemical filter system with an excellent penetration flux porous Ti/SnO<sub>2</sub>-Sb filter for efficient contaminant removal from water. *RSC Adv.* **2018**, *8*, 13933–13944. [[CrossRef](#)]
30. Liu, Z.; Zhu, M.; Zhao, L.; Deng, C.; Ma, J.; Wang, Z.; Liu, H.; Wang, H. Aqueous tetracycline degradation by coal-based carbon electrocatalytic filtration membrane: Effect of nano antimony-doped tin dioxide coating. *Chem. Eng. J.* **2017**, *314*, 59–68. [[CrossRef](#)]
31. Gao, G.; Zhang, Q.; Vecitis, C.D. CNT-PVDF composite flow-through electrode for single-pass sequential reduction–oxidation. *J. Mater. Chem. A* **2014**, *2*, 6185–6190. [[CrossRef](#)]
32. Peng, L.; Liu, H.; Wang, W.-L.; Xu, Z.-B.; Ni, X.-Y.; Wu, Y.-H.; Wu, Q.-Y.; Hu, H.-Y. Degradation of methylisothiazolinone biocide using a carbon fiber felt-based flow-through electrode system (FES) via anodic oxidation. *Chem. Eng. J.* **2020**, *384*, 123239. [[CrossRef](#)]

33. Yu, S.; Gao, Y.; Khan, R.; Liang, P.; Zhang, X.; Huang, X. Electrospun PAN-based graphene/SnO<sub>2</sub> carbon nanofibers as anodic electrocatalysis microfiltration membrane for sulfamethoxazole degradation. *J. Membr. Sci.* **2020**, *614*, 118368. [[CrossRef](#)]
34. Nataraj, S.; Yang, K.; Aminabhavi, T. Polyacrylonitrile-based nanofibers—A state-of-the-art review. *Prog. Polym. Sci.* **2012**, *37*, 487–513. [[CrossRef](#)]
35. Li, X.; Shao, S.; Yang, Y.; Mei, Y.; Qing, W.; Guo, H.; Peng, L.E.; Wang, P.; Tang, C.Y. Engineering interface with a one-dimensional RuO<sub>2</sub>/TiO<sub>2</sub> heteronanostructure in an electrocatalytic membrane electrode: Toward highly efficient micropollutant decomposition. *ACS Appl. Mater. Interfaces* **2020**, *12*, 21596–21604. [[CrossRef](#)] [[PubMed](#)]
36. Liu, H.; Cao, C.-Y.; Wei, F.-F.; Huang, P.-P.; Sun, Y.-B.; Jiang, L.; Song, W.-G. Flexible macroporous carbon nanofiber film with high oil adsorption capacity. *J. Mater. Chem. A* **2014**, *2*, 3557–3562. [[CrossRef](#)]
37. Xie, L.; Shu, Y.; Hu, Y.; Cheng, J.; Chen, Y. SWNTs-PAN/TPU/PANI composite electrospun nanofiber membrane for point-of-use efficient electrochemical disinfection: New strategy of CNT disinfection. *Chemosphere* **2020**, *251*, 126286. [[CrossRef](#)] [[PubMed](#)]
38. Li, W.; Zeng, L.; Yang, Z.; Gu, L.; Wang, J.; Liu, X.; Cheng, J.; Yu, Y. Free-standing and binder-free sodium-ion electrodes with ultralong cycle life and high rate performance based on porous carbon nanofibers. *Nanoscale* **2014**, *6*, 693–698. [[CrossRef](#)] [[PubMed](#)]
39. Li, X.; Zhou, M.; Wang, J.; Ge, F.; Zhao, Y.; Komarneni, S.; Cai, Z. Flexible and internal series-connected supercapacitors with high working voltage using ultralight porous carbon nanofilms. *J. Power Sources* **2017**, *342*, 762–771. [[CrossRef](#)]
40. Tang, Y.; Li, N.; Liu, A.; Ding, S.; Yi, C.; Liu, H. Effect of spinning conditions on the structure and performance of hydrophobic PVDF hollow fiber membranes for membrane distillation. *Desalination* **2012**, *287*, 326–339. [[CrossRef](#)]
41. Trellu, C.; Chaplin, B.P.; Coetsier, C.; Esmilaire, R.; Cerneaux, S.; Causserand, C.; Cretin, M. Electro-oxidation of organic pollutants by reactive electrochemical membranes. *Chemosphere* **2018**, *208*, 159–175. [[CrossRef](#)]
42. Liu, K.; Chen, L.; Chen, Y.; Wu, J.L.; Zhang, W.Y.; Chen, F.; Fu, Q. Preparation of polyester/reduced graphene oxide composites via in situ melt polycondensation and simultaneous thermo-reduction of graphene oxide. *J. Mater. Chem.* **2011**, *21*, 8612–8617. [[CrossRef](#)]
43. Arbab, S.; Teimoury, A.; Mirbaha, H.; Adolphe, D.C.; Noroozi, B.; Nourpanah, P. Optimum stabilization processing parameters for polyacrylonitrile-based carbon nanofibers and their difference with carbon (micro) fibers. *Polym. Degrad. Stab.* **2017**, *142*, 198–208. [[CrossRef](#)]
44. Zhang, L.; Aboagye, A.; Kelkar, A.D.; Lai, C.; Fong, H. A review: Carbon nanofibers from electrospun polyacrylonitrile and their applications. *J. Mater. Sci.* **2014**, *49*, 463–480. [[CrossRef](#)]
45. Yu, M.; Xu, Y.; Wang, C.; Hu, X.; Zhu, B.; Qiao, K.; Yuan, H. Heredity and difference of multiple-scale microstructures in PAN-based carbon fibers and their precursor fibers. *J. Appl. Polym. Sci.* **2012**, *125*, 3159–3166. [[CrossRef](#)]
46. Xu, W.; Xin, B.; Yang, X. Carbonization of electrospun polyacrylonitrile (PAN)/cellulose nanofibril (CNF) hybrid membranes and its mechanism. *Cellulose* **2020**, *27*, 3789–3804. [[CrossRef](#)]
47. Li, X.; Wang, J.; Zhao, Y.; Ge, F.; Komarneni, S.; Cai, Z. Wearable solid-state supercapacitors operating at high working voltage with a flexible nanocomposite electrode. *ACS Appl. Mater. Interfaces* **2016**, *8*, 25905–25914. [[CrossRef](#)]
48. Yang, T.; Du, M.; Zhu, H.; Zhang, M.; Zou, M. Immobilization of Pt nanoparticles in carbon nanofibers: Bifunctional catalyst for hydrogen evolution and electrochemical sensor. *Electrochim. Acta* **2015**, *167*, 48–54. [[CrossRef](#)]
49. Li, X.; Xiao, C.; Ruan, X.; Hu, Y.; Zhang, C.; Cheng, J.; Chen, Y. Enrofloxacin degradation in a heterogeneous electro-Fenton system using a tri-metal-carbon nanofibers composite cathode. *Chem. Eng. J.* **2022**, *427*, 130927. [[CrossRef](#)]
50. Xie, T.; Hu, H.; Chen, D.; Sun, P. Electrochemical degradation of tetracycline hydrochloride in aqueous medium by (B4C/C)-β-PbO<sub>2</sub> electrode. *Bull. Korean Chem. Soc.* **2017**, *38*, 756–762. [[CrossRef](#)]
51. Zhang, H.; Liu, F.; Wu, X.; Zhang, J.; Zhang, D. Degradation of tetracycline in aqueous medium by electrochemical method. *Asia-Pac. J. Chem. Eng.* **2009**, *4*, 568–573. [[CrossRef](#)]
52. Schnoor, M.H.; Vecitis, C.D. Quantitative examination of aqueous ferrocyanide oxidation in a carbon nanotube electrochemical filter: Effects of flow rate, ionic strength, and cathode material. *J. Phys. Chem. C* **2013**, *117*, 2855–2867. [[CrossRef](#)]
53. Yang, S.; Liu, Y.; Shen, C.; Li, F.; Yang, B.; Huang, M.; Yang, M.; Wang, Z.; Sand, W. Rapid decontamination of tetracycline hydrolysis product using electrochemical CNT filter: Mechanism, impacting factors and pathways. *Chemosphere* **2020**, *244*, 125525. [[CrossRef](#)] [[PubMed](#)]
54. Panizza, M.; Cerisola, G. Direct and mediated anodic oxidation of organic pollutants. *Chem. Rev.* **2009**, *109*, 6541–6569. [[CrossRef](#)] [[PubMed](#)]
55. Wang, J.; Zhi, D.; Zhou, H.; He, X.; Zhang, D. Evaluating tetracycline degradation pathway and intermediate toxicity during the electrochemical oxidation over a Ti/Ti<sub>4</sub>O<sub>7</sub> anode. *Water Res.* **2018**, *137*, 324–334. [[CrossRef](#)] [[PubMed](#)]